Published in final edited form as:
Biochem Biophys Res Commun. 2011 April 1; 407(1): 63–67. doi:10.1016/j.bbrc.2011.02.104.

Direct Observation of Chemokine Receptors 5 on T-lymphocyte Cell Surfaces Using Fluorescent Metal Nanoprobes 2: Approximation of CCR5 Populations

Jian Zhang[1], **Yi Fu**[1], **Ge Li**[2], **Richard Y. Zhao**[2,3,4], and **Joseph R. Lakowicz**[1]

[1] Center for Fluorescence Spectroscopy, University of Maryland School of Medicine, Department of Biochemistry and Molecular Biology, 725 West Lombard Street, Baltimore, MD 21201

[2] Division of Molecular Pathology, Department of Pathology, University of Maryland School of Medicine, 10 South Pine Street, Baltimore, MD 21201

[3] Department of Microbiology-Immunology, University of Maryland School of Medicine, 10 South Pine Street, Baltimore, MD 21201

[4] Institute of Human Virology, University of Maryland School of Medicine, 10 South Pine Street, Baltimore, MD 21201

Abstract

Metal nanoparticle probes were used as molecular imaging agents to detect the expression levels and spatial distributions of the CCR5 receptors on the cell surfaces. Alexa Fluor 647-labeled anti-CCR5 monoclonal antibodies (mAbs) were covalently bound to 20 nm silver nanoparticles to synthesize the mAb-metal complexes. We measured the single nanoparticle emission of the mAb-metal complexes, showing that the complexes displayed enhanced intensities and reduced lifetimes in comparison with the metal-free mAbs. Six HeLa cell lines with various CCR5 expressions were incubated with the mAb-metal complexes for the target-specific binding to the cell surfaces. Fluorescence cell images were recorded on a time-resolved confocal microscopy. The collected images expressed clear CCR5 expression-dependent optical properties. Two regression curves were obtained on the basis of the emission intensity and lifetime over the entire cell images against the number of the CCR5 expression on the cells. The emission from the single mAb-metal complexes could be distinctly identified from the cellular autofluorescence on the cell images. The CCR5 spatial distributions on the cells were analyzed on the cell images and showed that the low-expression cells have the CCR5 receptors as individuals or small clusters but the high expression cells have them as the dense and discrete clusters on the cell surfaces.

Keywords

Chemokine receptor 5 (CCR5); HeLa cell; CCR5 expression; anti-CCR5 monoclonal antibody (mAb); Alexa Fluor 647; mAb-metal complexes; lifetime-resolved cell imaging; metal-enhanced fluorescence (MEF); plasmon-coupled probes (PCPs)

Corresponding author information: jian@cfs.umaryland.edu, Tel: 410-706-7500, Fax: 410-706-8409.

Introduction

The chemokine receptor 5 (CCR5) is a membrane protein that can be recognized by its R5 HIV virus during early stages of infection [1,2]. CXCR4 is another well-known co-receptor that can be recognized by X4 virus during late stage infection [3,4]. During a HIV-1 viral infection, the viral envelope glycoprotein gp120 is first in contact with a cellular receptor CD4 on T-lymphocyte followed by interaction with a coreceptor such as CCR5 and CXCR4 [5]. The expression level of CCR5 or CXCR4 on the cells thus is important in the probability of personal infection by HIV-1 virus. On the other hand, the expression amounts of these coreceptors often vary, and the virologic significance of such variations is still unclear [6,7]. It is important to determine the expression of coreceptors on the cell surfaces. In addition, the distributions of coreceptors on the cells are expected to influence the viral infections [8]. It thus is important to be able to directly observe the distributions of coreceptors on the cell surfaces.

Fluorescence cell imaging is an important method to detect the target molecules in the cells [9,10]. However, such measurements are also limited by drawbacks of imaging agents that are mostly composed of conventional organic fluorophores [11,12]. In order to improve the optical properties, several groups have reported on the nanoparticle imaging agents during past years [13–19]. We are interested in the metal nanoparticle probes because of their significant improvements on the optical properties of attached organic fluorophores. These metal nanoparticle probes are made by conjugating the organic fluorophores onto the metal nanoparticles with diameters ranging from 10 to 100 nm [13–19]. The interactions between the fluorophores and plasmon resonances arising from the metal nanoparticles occur in the near-field resulting in enhanced emission brightness and increased photostability [20–23]. Importantly, the lifetime of fluorophore is also reduced to a unique shortened value that can be used to distinguish the probe emission signals from the cellular autofluorescence by lifetime-resolved cell imaging [24]. In a recent report, we developed the metal nanoparticle probes for the observations of presence and distribution of the CCR5 receptors on CD4(+) T-lymphocytic cells [25]. However, the results were only semi-quantitative because the CCR5 receptors were densely populated on the cell surfaces and the emission from the single probes could not be resolved. In another report, we found that the optical properties over the entire cell images including the intensity and lifetime depended upon the total number of metal nanoparticle probes on the cells [26]. Based on the previous reports, we now describe a quantitative approach that can correlate the optical properties over the cell images with the expression of the CCR5 receptors on the cells. We expect that this approach will allow us to determine the CCR5 populations accurately on the cells with unknown expression levels. In addition, we intend to observe the single CCR5 receptors distributed through the cell surfaces. These observations can be potentially used to investigate the molecular mechanism of HIV infection.

Materials and Methods

All reagents and spectroscopic grade solvents were from Sigma-Aldrich. Alexa Fluor 647 succinimidyl ester and Alexa Fluor 647 goat anti-mouse IgM were from Invitrogen. Nanopure water (>18.0 MΩ.cm) was obtained using the Millipore Milli-Q gradient system. The (2-mercapto-propionylamino) acetic acid 2,5-dioxo-pyrrolidin-1-ylester was synthesized in a method as described previously [25]. Monoclonal CCR5 antibody (45531) was obtained from the NIH AIDS Research and Reference Reagent Program.

Preparation of Fluorescent mAb-metal complex

Anti-CCR5 mAbs were fluorescently labeled with Alexa Fluor 647 via the reactive ester reaction [27]. 20 nm silver nanoparticles were synthesized by reduction of silver nitrate with

ascorbic acid [25]. The silver nanoparticles were coated with monolayers of hexa(ethylene glycol)mono-11-(acetythio)undecyl ether [28], and then partially substituted by (2-mercapto-propionylamino) acetic acid 2,5-dioxo-pyrrolidin-1-ylester via a ligand exchange reaction [28]. These silver nanoparticles were co-dissolved with the labeled mAb in 10 mM PBS buffer solution at pH 8.0 and the solution was continuously stirred for 2 h at 4°C. The mAb-metal complexes were recovered by centrifugation and then dispersed in 10 mM PBS buffer solution at pH 7.4.

Cell culture and immuno-conjugation

Six HeLa cell lines that have different CCR5 expression levels on the membranes were selected for the experiments. The cells were grown in Dulbecco's modified Eagle medium supplemented with 10% fetal bovine serum [29]. Based on flow cytometry measurements, these cell lines were found to have CCR5 receptors of 0, 700, 2,000, 9,000, 20,000, and 50,000 receptors per cell. The cell lines were incubated with the mAb-metal complexes for the immuno-reaction with the CCR5 receptors on the cells. Typically, the HeLa cells on the coverslips were incubated with 0.5 nM mAb-metal complex for 2 h [25], washed with the PBS-Mg solution, and dried in air for cell imaging. As controls, the cell lines were also incubated with the metal free labeled mAbs under the same conditions.

Ensemble spectral measurements, cell imaging, TEM measurement

Absorption spectra were measured with a Hewlett Packard 8453 spectrophotometer. Ensemble fluorescence spectra were recorded with a Cary Eclipse Fluorescence Spectrophotometer. The imaging measurements were carried out on a time-resolved scanning confocal microscopy (MicroTime 200, PicoQuant). The measurement system consists of an inverted confocal microscope coupled to a high-sensitivity detection setup. A single mode pulsed laser diode (635 nm, 100 ps, 40 MHz) (PDL800, PicoQuant) was used for the excitation light. An oil immersion objective (Olympus, 100×, 1.3NA) was used both for focusing laser light onto sample and collecting fluorescence emission. The emission signal that passed a dichroic mirror was focused onto a 75 μm pinhole for spatial filtering to reject out-of-focus signal and recorded on a single photon avalanche diode (SPAD) (SPCM-AQR-14, Perkin Elmer Inc). Bandpass filters were used to eliminate the excitation scattering and to minimize spectral crosstalk. The data collected with a TimeHarp 200 board were stored in the Time-Tagged Time-Resolved Mode (TTTR), which allows recording of every photon with its individual timing and detection channel information.

Transmission electron micrographs (TEM) were taken with a side-entry Philips electron microscope at 120 keV. Samples were cast from water solutions onto standard carbon-coated (200–300 Å) Formvar films on copper grids (200 mesh) by placing a droplet of a 1 mg/mL aqueous sample solution on grids. The size distribution of metal core was analyzed with Scion Image Beta Release 2 counting at least 200 particles.

Results and Discussion

Anti-CCR5 mAbs were fluorescently labeled by Alexa Fluor 647 [27]. From the absorbance spectrum of labeled mAb and the extinct coefficient of Alexa Fluor 647, it was estimated that each mAb molecule was on average labeled by 4.3 fluorophores. Upon excitation at 630 nm, the labeled mAbs exhibited a maximal emission at 670 nm, close to free Alexa Fluor 647.

The silver nanoparticles were found to have a relatively homogeneous size distribution of 20±10 nm [25]. The absorbance spectrum of silver nanoparticles showed a plasmon resonance centered at 415 nm. These metal nanoparticles were coated by monolayers of

organic ligands on the metal surfaces to increase their chemical stability in buffer solution. To covalently bind the mAb molecules, the nanoparticles were partially substituted with (2-mercapto-propionylamino) acetic acid 2,5-dioxo-pyrrolidin-1-ylester via a ligand exchange reaction [28] followed by codissolving with the labeled mAbs in buffer solution [26]. The metal nanoparticles were collected by centrifugation and the spectral measurements showed an emission maximum at 667 nm corresponding to Alexa Fluor 647 (Figure S1), indicating the mAbs were indeed bound to the silver nanoparticles. The mAb-metal complexes were validated by absorbance spectrum (Figure S1) showing a silver plasmon resonance at 417 nm almost identical to the as-prepared silver nanoparticles, implying that the metal nanoparticles were not significantly altered or aggregated during the surface reactions. The TEM images (inset of Figure S1) were essentially the same as the profiles of the individual nanoparticles. By a NaCN treatment which removed the silver, the number of bound mAb on each metal nanoparticle was measured to be 11.5 [26,30].

The optical properties of single mAb-metal complexes as well as metal-free mAbs were determined on a time-resolved confocal microscopy. We found that a typical time trace of a single mAb displayed a multiple-step photobleaching representing the presence of several fluorophores on a single mAb. In contrary, a time trace of a single mAb-metal complex displayed an exponential decay representing a single nanoparticle was bound by a number of the labeled mAbs (Figure 1). For each probe sample, at least 50 emission spots were collected for the histogram analysis (Figure S2). It was revealed that with the binding of labeled mAbs to the metal nanoparticles the average intensity was *approx*. 30-fold increased (Figure S2a) and the lifetime was dramatically decreased from 1.5 ns to 0.3 ns (Figure S2b) [23,24]. Based on the binding number of mAb on each metal nanoparticle, it appears that the fluorescence intensity of mAbs was increased about 4-fold by the silver nanoparticle. We also noticed that the lifetime of mAb-metal complexes was shorter than that of the cellular autofluorescence (2 – 5 ns). With enhanced emission intensity and reduced unique lifetime different from the cellular autofluorescence, the emission signals of mAb-metal complexes can be separated from the cellular backgrounds during lifetime-resolved cell imaging.

The chemical stability of the nanoparticle probes in cell culture media is always a concern [31]. The potential aggregation of the mAb-metal complexes in buffer or cell media were examined using TEM and absorbance spectra: both are sensitive to the metal particle-particle proximity [32]. The results showed insignificant aggregation, which we ascribed to the protection of metal surfaces by the organic monolayers and bound mAb molecules on their external surfaces.

The mAb-metal complexes were used as molecular imaging agents to bind with the CCR5 targets on the cells. Six HeLa cell lines with different CCR5 expression levels were selected to incubate with the mAb-metal complexes. As controls, the cell lines were also incubated with the metal-free labeled mAbs. The representative cell images are presented in Figure 2. We found that the blank unlabeled cells have dim images (Figure 2a) in comparison with the labeled mAbs-conjugated cells (Figure 2b), indicating that the mAbs have bound to the cells. We also noticed that for the mAbs-conjugated cells, the changes on the optical properties throughout the cell images could be detected but the emission signals from the single mAbs could not be resolved using either the intensity or lifetime measurement. This result is due to low emission intensities from the single mAbs and close lifetimes of the mAbs to the cellular autofluorescence.

The nanoparticle-conjugated cells showed much brighter images (Figure 2c–f) than the blank and mAb-conjugated cells. Importantly, the emission signals of single mAb-metal complexes could be distinctly isolated over the cellular backgrounds due to enhanced intensities and different lifetimes of the nanoparticle probes. The nanoparticle-conjugated

cells also displayed clearly CCR5 expression-dependent images. On the images with low CCR5 expression levels (Figure 4c–e), the emission signals of mAb-metal complexes could be identified as small and round individual spots, which presumably represented the single receptors or small CCR5 clusters. With increased CCR5 expression (Figure 4f–h), the emission signals of mAb-metal complexes appeared as discrete profiles throughout the cell images that may represent large CCR5 clusters.

We also tested the immuno-specificity of the mAb-metal complexes with the CCR5 targets on the cells. For this control experiment, Alexa Fluor 647 goat anti-mouse IgM molecules were covalently bound on the 20 nm silver nanoparticles. These IgG mAb-metal complexes are not expected to bind to the cell surfaces. The IgM-metal complexes were incubated with the highest CCR5 expression HeLa cells. The collected cell images showed on average less than 10 emission spots from the IgM-metal complexes demonstrating the immuno-specificity of CCR5 mAb-Ag complexes with the target CCR5 receptors on the cell surfaces.

For each cell sample, at least 20 cell images were collected to analyze the CCR5 expression-dependent optical properties over the cell images. Using PicoQuant analysis software, the emission intensities and lifetimes were presented as the histograms in Figure 3. In comparison with the blank unlabeled cells, the nanoparticle-conjugated cells showed a higher emission intensity accompanying with an increase at high intensity range (Figure 3a). Meanwhile, the lifetime of the nanoparticle-conjugated cells showed a shift to a shorter value around 0.5 ns (Figure 3b). Considering that the emission of the blank unlabeled cells is completely from the cellular autofluorescence, the changes on the optical properties over the cell images were due to the conjugations of mAb-metal complexes on the cells. Compared with the nanoparticle-conjugated cells, the mAb-conjugated cells showed much smaller changes in the optical properties over the cell images including intensity and lifetime (Figure 3), which were principally due to relatively weak emission signals from the metal-free mAbs. It was also noticed that the lifetime values from the nanoparticle-conjugated cells and the blank unlabeled cells did not overlap (Figure 3a) whereas the lifetime values from the mAb-conjugated cells and the blank unlabeled cells overlapped significantly (Figure 3b). This is the reason that the emission from the mAb-metal complexes can be resolved from the cellular autofluorescence but the emission from mAbs cannot be resolved in the lifetime-resolved cell imaging. Therefore, the mAb-metal complexes are regarded as more valuable molecular imaging agents for detecting the single CCR5 receptors on the cells.

For the nanoparticle-conjugated cells, the average emission intensity and lifetime over the cell images were found to strongly rely on the number of mAb-metal complexes on the cells [26]. The average intensity and lifetime were estimated from the maximal values of histograms for at least 20 cell images, and plotted against the expression numbers of CCR5 on the cells, respectively (Figure 4a and b). The regression curves on the intensity showed a significant increase with the CCR5 expression number whereas the regression curves on the lifetime showed a decrease. Both curves were created on the basis of cells with known amounts of CCR5. We expect to use the regression curves for the estimation of the expression numbers of CCR5 on the cells with unknown amounts of receptors.

The observation of spatial distributions of CCR5 on the cells is another important objective in this research. To reduce the interference from the cellular autofluorescence, the emission data with the lifetimes over 1.5 ns were removed from the images of nanoparticle-conjugated cells using OriginPro 7.0 software. The residuals were regarded primarily from the mAb-metal complexes on the cells. On the images of cells with the low CCR5 expressions (three cell lines: 0, 700, and 2,000), the emission from the mAb-metal complexes could be clearly isolated as individual spots and the numbers could be precisely

counted to be on average *approx*. 6, 150, and 400, respectively (Figure S3). We realize that these count numbers are significantly lower than the expected expression numbers, which may be due to two reasons. First, the mAb-metal complexes are bound with multiple mAbs per metal nanoparticle so that a single mAb-metal complex can immuno-interact with more than one CCR5 receptor on the cell. Second, the x-y dimensional resolution of the confocal microscopy is 200 × 200 nm which is much larger than the size of mAb-metal complex. As a result, one emission spot on the cell image may contain the signals from several mAb-metal complexes that cannot be resolved. Using the actual CCR5 expression numbers as references, we estimate that a single emission spot on the cell image may represent approx. 5 CCR5 receptors on the cell surface.

Unlike the low-expression cells, the high-expression cells showed the emission of mAb-metal complexes distributed in clusters throughout the cell images. Thus, the number of emission spots on the cell images could not be counted. However, the cell images still provided useful information for evaluation to the distributions of CCR5 throughout the cells, and showed the coverage percentage of CCR5 over the total cell. For this analysis, we integrate the total lifetime data as total cell area and the lifetime data shorter than 1.5 ns as the occupation area of mAb-metal complexes on the cell. In actual treatments, the total lifetime data on the cell image were normalized to 1 followed by integration. The obtained value can represent the entire area of cell. The lifetime data over 1.5 ns were subsequently removed and the residuals were normalized to 1 followed by integration. This value may represent the occupation area of mAb-metal complexes on the cell. The ratio of two values is taken to represent the coverage percentage of CCR5 occupation over the cell surface. The ratios from the different cell lines were estimated and plotted against the actual numbers on the cells (Figure S4) to obtain a regression curve showing a rapid increase at low expression and a slow increase at high expression, consistent with the regression curve on the emission intensity (Figure 4a). For the cell line with the highest expression of 50,000, the coverage percentage was close to 0.5, suggesting that the majority of CCR5 receptors were distributed as dense and discrete clusters on about 50% area of the overall cell surfaces.

Supplementary Material

Refer to Web version on PubMed Central for supplementary material.

Acknowledgments

The authors would like to thank Drs. Alonso Heredia and Robert Redfield for the CCR5-positive HeLa cell lines. This research was supported by grants from NIH (EB009509, HG-002655, GM091081, RR026370, and CA134386).

References

1. Dragic T, Litwin V, Allaway GP, Martin SR, Huang YX, Nagashima KA, Cayanan C, Maddon PJ, Koup RA, Moore JP, Paxton WA. HIV-1 entry into CD4+ cells is mediated by the chemokine receptor CC-CKR-5. Nature. 1996; 381:667–673. [PubMed: 8649512]
2. Gorry PR, Holm GH, Mehle A, Morgan T, Cayabyab M, Farzan M, Wang H, Bell JE, Kunstman K, Moore JP, Wolinsky SM, Gabuzda D. Increased CCR5 affinity and reduced CCR5/CD4 dependence of a neurovirulent primary human immunodeficiency virus type 1 isolate. J Virol. 2002; 76:6277–6292. [PubMed: 12021361]
3. Thompson, Cormier CE, Dragic T. CCR5 and CXCR4 usage by non-clade B human immunodeficiency virus type 1 primary isolates. J Virol. 2002; 76:3059–3064. [PubMed: 11861874]

4. Trkola A, Matthews J, Gordon C, Ketas T, Moore J. A cell line-based neutralization assay for primary human immunodeficiency virus type 1 isolates that use either the CCR5 or the CXCR4 coreceptor. J Virol. 1999; 73:8966–8974. [PubMed: 10516002]
5. Lusso P. HIV and the chemokine system: 10 years later. Embo J. 2006; 25:447–456. [PubMed: 16437164]
6. Agrawal L, Lu X, Qingwen J, VanHorn-Ali Z, Nicolescu IV, McDermott DH, Murphy PM, Alkhatib G. Role for CCR5Delta32 protein in resistance to R5, R5X4, and X4 human immunodeficiency virus type 1 in primary CD4+ cells. J Virol. 2004; 78:2277–2287. [PubMed: 14963124]
7. Huang Y, Paxton WA, Wolinsky SM, Neumann AU, Zhang L, He T, Kang S, Ceradini D, Jin Z, Yazdanbakhsh K, Kunstman K, Erickson D, Dragon E, Landau NR, Phair J, Ho DD, Koup RA. The role of a mutant CCR 5 allele in HIV-1 transmission and disease progression. Nat Med. 1996; 2:1240–1243. [PubMed: 8898752]
8. Martinson JJ, Chapman NH, Rees DC, Liu YT, Clegg JB. Global distribution of the CCR5 gene 32-basepair deletion. Nat Genet. 1997; 16:100–103. [PubMed: 9140404]
9. Berezin MY, Achilefu S. Fluorescence lifetime measurements and biological imaging. Chem Rev. 2010; 110:2641. [PubMed: 20356094]
10. Kobayashi H, Ogawa M, Alford R, Choyke PL, Urano Y. Target-cancer-cell-specific activatable fluorescence imaging probes: rational design and in vivo applications. Chem Rev. 2010; 110:2620. [PubMed: 20000749]
11. Licha K, Riefke B, Ntziachristos V, Becker A, Chance B, Semmler W. Hydrophilic cyanine dye as contrast agents for near-infrared tumor imaging: synthesis, photophysical properties and spectroscopic in vivo characterization. Photochem Photobiol. 2000; 72:392–398. [PubMed: 10989611]
12. Lakowicz, JR. Principles of fluorescence spectroscopy. 3. Kluwer Academic/Plenum Published; New York: 2006.
13. Sokolov K, Chumanov G, Cotton TM. Enhancement of molecular fluorescence near the surface of colloidal metal films. Anal Chem. 1998; 70:3898–3905. [PubMed: 9751028]
14. Hubert C, Rumyantseva A, Lerondel G, Grand J, Kostcheev S, Billot L, Vial A, Bachelot R, Royer P, Chang SH, Gray SK, Wiederrecht GP, Schatz GC. Near-field photochemical imaging of noble metal nanostructures. Nano Lett. 2005; 5:615–619. [PubMed: 15826096]
15. Jain K, Huang X, El-Sayed IH, El-Sayed MA. Noble metals on the nanoscale: optical and photothermal properties and applications in imaging, sensing, biology, and medicine. Acc Chem Res. 2008; 41:1578–1586. [PubMed: 18447366]
16. Ghosh SK, Pal T. Interparticle Coupling effect on the surface plasmon resonance of gold nanoparticles: from theory to applications. Chem Rev. 2007; 107:4797. [PubMed: 17999554]
17. Kamat PV. Photophysical, photochemical and photocatalytic aspects of metal nanoparticle. J Phys Chem B. 2002; 106:7729–7744.
18. He GS, Tan LS, Zheng Q, Prasad PN. Multiphoton absorbing materials: molecular designs, characterizations, and applications. Chem Rev. 2008; 108:1245–1330. [PubMed: 18361528]
19. Schwartzberg AM, Zhang JZ. Novel optical properties and emerging applications of metal nanostructures. J Phys Chem C. 2008; 112:10323–10337.
20. Stoermer R, Keating CD. Distance-dependent emission from dye-labeled oligonucleotides on striped Au/Ag nanowires: effect of secondary structure and hybridization efficiency. J Am Chem Soc. 2006; 128:13243–13254. [PubMed: 17017805]
21. Zhang J, Fu Y, Chowdry MH, Lakowicz JR. Single molecule studies on fluorescently labeled silver particles: effects of particle size. J Phys Chem C. 2008; 112:18–26.
22. Lakowicz JR. Radiative Decay Engineering: Biophysical and Biomedical Applications. Anal Biochem. 2001; 298:1–24. [PubMed: 11673890]
23. Lakowicz JR. Radiative decay engineering 5: metal-enhanced fluorescence and plasmon emission. Anal Biochem. 2005; 337:171–194. [PubMed: 15691498]
24. Zhang J, Fu Y, Li G, Zhao RY, Lakowicz JR. Direct observation to chemokine receptor 5 on T-lymphocyte cell surface using fluorescent metal nanoprobes. Biochem Biophys Res Comm. 2010; 400:111–116. [PubMed: 20705055]

25. Zhang J, Fu Y, Liang D, Nowaczyk K, Zhao RY, Lakowicz JR. Single cell fluorescence imaging using metal plasmon-coupled probe 2: lifetime image and single molecule counting. Nano Lett. 2008; 8:1179–1186. [PubMed: 18341300]

26. Zhang J, Fu Y, Liang D, Zhao RY, Lakowicz JR. Fluorescent avidin-bound silver particle: a strategy for single target molecule detection on a cell membrane. Anal Chem. 2009; 81:883–889. [PubMed: 19113832]

27. Brinkley MA. brief survey of methods for preparing protein conjugates with dyes, haptens and crosslinking reagents. Bioconj Chem. 1992; 3:2–13.

28. Templeton AC, Wuelfing WP, Murray RW. Monolayer-protected cluster molecules. Acc Chem Res. 2000; 33:27–36. [PubMed: 10639073]

29. Platt EJ, Wehrly K, Kuhmann SE, Chesebro B, Kabat D. Effects of CCR5 and CD4 cell surface concentrations on infections by macrophagetropic isolates of human immunodeficiency virus type 1. J Virol x. 1998; 72:2855–2864.

30. Rosi NL, Mirkin CA. Nanostructures in biodiagnostics. Chem Rev. 2005; 105:1547–1562. [PubMed: 15826019]

31. Riley T, Govender T, Stolnik S, Xiong CD, Garnett MC, Illum L, Davis SS. Colloidal stability and drug incorporation aspects of micellar-like PLA-PEG nanoparticles Colloids and Surfaces. B: Biointerfaces. 1999; 16:147–159.

32. Burt JL, Gutiérrez-Wing C, Miki-Yoshida M, José-Yacamán M. Interaction of silver nanoparticles with HIV-1. Langmuir. 2004; 20:11778–11783. [PubMed: 15595811]

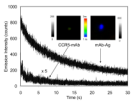

Figure 1.
Representative time traces of single labeled anti-CCR5 mAb and mAb-metal complex upon excitation at 635 nm. The insets represent the respective typical fluorescence images of them in the both emission intensity and lifetime. The scales of diagrams are 5 × 5 μm and the resolutions are 100 × 100 pixel with an integration of 0.6 ms/pixel.

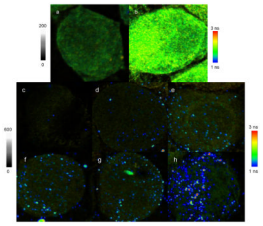

Figure 2.
Representative cell emission intensity and lifetime images: (a) an image of blank cell without labeling and (b) an image of mAbs-conjugated cell with the expression number of 50,000 CCR5. Images of (c)–(h) represent those from the cells with different CCR5 expressions: (c) 0, (d) 700, (e) 2,000, (f) 9,000, (g) 20,000, and (h) 50,000. These cells were incubated with the mAb-metal complexes, respectively. The scales of diagrams are 50 × 50 μm and the resolutions are 500 × 500 pixel with an integration of 0.6 ms/pixel. Notice that the images of (c)–(h) have different intensity bars from the images of (a)–(b).

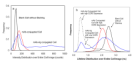

Figure 3.
Distributions of (a) average emission intensity and (b) average lifetime over the entire whole cell images. Blank cells without labeling, mAbs-conjugated cells with the expression umber of 50,000, PCF-conjugated cells with low (2,000) or high (50,000) copies of CCR5. The cells with 50,000 copies were shown in (a). Two different HeLa cell lines with low (2,000) or high (50,000) copies were shown in (b) to compare distributions for different treatments.

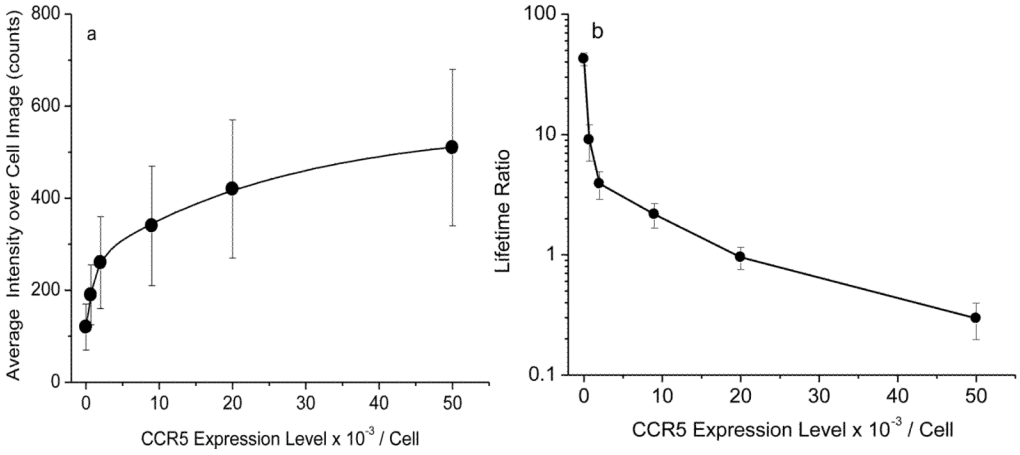

Figure 4.

Dependence of (a) average emission intensity and (b) average lifetime over the entire cell images on the expression numbers of CCR5 on the cell surfaces.